

# Gating of the HypoPP-1 mutations: I. Mutant-specific effects and cooperativity

Alexey Kuzmenkin · Chao Hang · Elza Kuzmenkina · Karin Jurkat-Rott

Received: 11 October 2006 / Revised: 15 December 2006 / Accepted: 29 January 2007 / Published online: 27 February 2007  
© Springer-Verlag 2007

**Abstract** Hypokalemic periodic paralysis type 1 (HypoPP-1) is a hereditary muscular disorder caused by point mutations in the gene encoding the voltage-gated  $\text{Ca}^{2+}$  channel  $\alpha$  subunit ( $\text{Ca}_v1.1$ ). Despite extensive research, the results on HypoPP-1 mutations are minor and controversial, as it is difficult to analyse  $\text{Ca}^{2+}$  channel activation macroscopically due to an existence of two open states. In this study, we heterologously expressed the wild-type and HypoPP-1 mutations introduced into the rabbit cardiac  $\text{Ca}^{2+}$  channel (R650H, R1362H, R1362G) in HEK-293 cells. To examine the cooperative effects of the mutations on channel gating, we expressed two double mutants (R650H/R1362H, R650H/R1362G). We performed whole-cell patch-clamp and, to obtain more information, applied a global fitting procedure whereby several current traces elicited by different potentials were simultaneously fit to the kinetic model containing four closed, two open and two inactivated states. We found that all HypoPP-1 mutations have “loss-of-function” features: D4/S4 mutations shift the equilibrium to the closed states, which results in reduced open probability, shorter openings and, therefore, in smaller currents, and the D2/S4 mutant slows the activation. In addition, HypoPP-1 histidine mutants favored the second open state  $O_2$  with a possibly lower channel selectivity. Cooperativity between the D2/S4 and D4/S4 HypoPP-1 mutations manifested in dominant effects of the

D4/S4 mutations on kinetics of the double mutants, suggesting different roles of D2/S4 and D4/S4 voltage sensors in the gating of voltage-gated calcium channels.

**Keywords** Hypokalemic periodic paralysis · L-type calcium channels · Global fitting · Gating model · Double-mutant cycle analysis · Channel selectivity

## Introduction

Hypokalemic periodic paralysis (HypoPP) is an autosomal dominant skeletal muscle disorder characterised by spontaneous weakness and low potassium serum level during paralytic attacks (for review, see [27]). HypoPP is caused by mutations in the genes encoding the skeletal muscle voltage-gated  $\text{Ca}^{2+}$  channel  $\text{Ca}_v1.1$   $\alpha_1$  subunit (HypoPP-1) [21, 35] and the voltage-gated  $\text{Na}^+$  channel  $\text{Na}_v1.4$   $\alpha$  subunit (HypoPP-2) [4, 22]. The mutations are located in the fourth transmembrane segments either of the second domain (D2/S4, HypoPP-2) or of the second and fourth (D2/S4, D4/S4, HypoPP-1) domains of the corresponding channels and are replacements of a positively charged arginine by a neutral amino acid. As the S4 transmembrane segments are suggested to act as voltage sensors opening the channel gate upon membrane depolarisation [41], the effects of HypoPP mutations are of interest to understand the disease pathogenesis and voltage-dependent gating of ion channels in general.

In case of HypoPP-2, the pathogenesis is partly elucidated. HypoPP-2 mutations decrease the current density, impair the activation and, most importantly, trap the channels in the inactivated states from which they cannot be reactivated [2, 22, 25, 40]. As the  $\text{Na}_v1.4$  are responsible for the initiation and propagation of action

Alexey Kuzmenkin and Chao Hang contributed equally to this work.

A. Kuzmenkin · C. Hang · E. Kuzmenkina · K. Jurkat-Rott (✉)  
Department of Applied Physiology, University of Ulm,  
89081 Ulm, Germany  
e-mail: karin.jurkat-rott@uni-ulm.de

A. Kuzmenkin (✉)  
Institute of Neurophysiology, University of Cologne,  
50931 Cologne, Germany  
e-mail: alexei21@hotmail.com

potentials in the skeletal muscle, the aforementioned changes impair sodium channel function and lead to a decrease in muscle excitability and, thus, to paralysis.

Much less is known about the pathophysiology of HypoPP-1 caused by mutations in  $Ca_v1.1$  channels, which function as the voltage sensors of the calcium release channels of the sarcoplasmic reticulum, and initiate muscle contraction. Previously, HypoPP-1 single mutations were studied electrophysiologically in various expression systems. The most prominent effect of HypoPP-1 mutations was a reduction of current density [26, 28, 31, 32]. Changes of steady-state and kinetic parameters of activation in HypoPP-1 mutants were controversial among different groups [23, 29–32] and even within the same group [31, 32]. The main reason for controversies was a different analysis of calcium channel gating. In contrast to other voltage-gated cation channels, calcium channels have a very pronounced second component of activation due to an existence of the second open state, characterised by long-lasting openings [9, 10, 14, 42]. However, all previous works on HypoPP-1 mutants did not take into account this characteristic feature of calcium channel gating, analyzing only peak amplitudes and single-exponential activation [23, 26, 29–32].

To resolve both components of calcium channel activation, we analyzed wild-type (WT) and HypoPP-1 channel kinetics by means of global fitting to gain insight into HypoPP-1 channel gating and S4 voltage sensor function. We demonstrated that the effects of the HypoPP-1 mutations on the two activation components are clearly different. The first component of activation, from the early closed to the first open state, is disfavored, suggesting the HypoPP-1 mutants to have “loss-of-function” features; however, differently realised for R650H and R1362H/G. The second activation component, reflecting transition to the second open state, is strongly stabilised in HypoPP-1 histidine mutants, resulting in a re-distribution of the open states. Additional analysis of the double mutants revealed dominant effects of the D4/S4 mutations on the kinetics of the double mutants. Our results give an insight into biophysical properties of HypoPP-1 mutations and suggest distinct functions of D2/S4 and D4/S4 voltage sensors in calcium channel gating.

## Materials and methods

### Mutagenesis

HypoPP-1 mutations analogous to R528H, R1239H and R1239G were introduced into rabbit cardiac calcium channel in pcDNA3 at the corresponding positions: R650H, R1362H and R1362G. In vitro site-directed mutagenesis was performed using QuikChange™ Site-Directed Mutagenesis Kit from STRATAGENE. Mutagenic primers were F: tgtgctgca

ctgcgtgctgctctg, R: gcacgcagtgc agcacagagatgccca for R650H; F: ctcttcgcctgttccacgtcatgcgctgtgcaagctg, R: cagcttgaccaggcgcgatgacgtggaacaggcggagaag for R1362H; F: ctcttcgcctgttctgggtcatgcgctgtgcaagctg, R: cagcttgacca ggcgatgaccccgaaacaggcggagaag for R1362G.

Two double mutations, R650H/R1362H (HH) and R650H/R1362G (HG) were constructed by exchanging fragments from the three single mutations (encoding R650H, R1362H and R1362G). Afl II and BstE II restriction endonucleases were selected to split the plasmid into two fragments. One was 10 kb and the other 2 kb. Ligating the 10 kb fragment from R650H separately with 2 kb fragments encoding R1362H or R1362G formed the double mutations.

### Cell culture and transfection

Human embryonic kidney 293 cells (HEK 293) were cultured in Dulbecco's modified Eagle's medium supplemented with 10% fetal calf serum in a humidified atmosphere (95%) at 5%  $CO_2$  and 37°C. Cells were used from 12–24 passages and were split every 4 days.

Transfection was performed using the standard calcium phosphate method. For calcium channel measurements, plasmids containing the rabbit cardiac calcium channel  $\alpha_1$  subunits were co-transfected at a ratio of 1:1:1 with those containing the rabbit cardiac calcium channel  $\beta_2$  subunit and CD8 receptor genes. Binding of CD8 antibody-coated beads was used as a visual marker to identify successfully transfected cells.

### Whole-cell recording and data analysis

Standard whole-cell recording technique [12] was applied for recording calcium channel currents. All recordings were performed using an Axopatch 200A patch-clamp amplifier linked to a personal computer with installed pCLAMP program (Axon Instruments, Foster City, CA, USA). Internal solutions contained (in mM): 142 CsCl, 1  $MgCl_2$ , 1 Mg-ATP, 10 EGTA, 5 HEPES; pH 7.4. The extracellular solution contained (in mM): 103 NMG, 5 CsCl, 1  $MgCl_2$ , 10 HEPES, 20  $BaCl_2$ ; pH 7.4. CsOH was used to change the pH values. All whole-cell recordings were performed at room temperature (20–22°C) with barium as charge carrier instead of calcium to avoid calcium-induced inactivation. Leak subtraction was not applied. Sampling interval was 120  $\mu s$ . Series resistance errors were <4 mV. Excel (Microsoft), pCLAMP and ORIGIN (Microcal Software, Northampton, MA, US) programs were used for displaying and analysing recordings. Data are presented as the mean  $\pm$  standard error of the mean (SEM). Student's *t* test was applied for statistical evaluation; the significance level was set at  $P < 0.05$ .

For a detailed picture of channel gating in the WT and mutants, we employed a global fitting procedure. This

method and the equations used for the calculation of basic channel parameters are described in Appendix A.

Analogues of the HypoPP-1 mutations are located in the functionally important parts of the  $\text{Ca}_v1.2$  channel: R650H—in the voltage sensor S4 of the second domain (D2/S4) and R1362H, R1362G mutations—in the voltage sensor S4 of the fourth domain (D4/S4). For estimation of cooperativity of the HypoPP-1 D2/S4 and D4/S4 mutations in the channel gating, we applied the double-mutant cycle analysis and calculated coupling energy between the corresponding mutations in equilibrium ( $\Delta G_{\text{coupling}}$ ) and in the forward and backward transitions ( $\Delta G_{\ddagger, \text{coupling}}$ ), as explained in Appendix B.

## Results

### Voltage sensitivity and current density are reduced in HypoPP-1 mutants

We studied three L-type cardiac calcium channel mutations homologous to the HypoPP-1 mutations: R650H in D2/S4, R1362H and R1362G in D4/S4. As the HypoPP-causing mutations are located in the different domains of the L-type calcium channel  $\alpha$  subunit, we evaluated the cooperative effects in two double mutations R650H/R1362H (HH) and R650H/R1362G (HG). For the macroscopic analysis of activation and for the detailed analysis of the calcium channel gating by kinetic simulations, we obtained current traces elicited by a family of depolarising pulses from a holding potential of  $-90$  mV to the test voltage from  $-60$  mV to  $+60$  mV in  $10$ -mV steps. Figure 1a shows the superimposed original current traces elicited by a selected test pulse of  $+10$  mV.

As the main goal of our study was to resolve the HypoPP-related changes of the activation pathway, we applied  $100$ -ms depolarising pulses. This short duration was necessary to prevent a run-down (amplitude decrease) of calcium channel currents and to minimise the fluctuations of the electric parameters (cell capacitance, pipette resistance) during the experiment, as the resulting current amplitude and kinetics changes would make the procedure of global fitting, applied in

this study, fully impossible. Therefore, inactivation rate constants could not be determined precisely and are not discussed.

To grossly compare the steady-state parameters of activation, we normalised the current amplitudes by the cell capacitance for each cell separately and plotted the means against the voltages tested (current–voltage ( $I$ – $V$ ) curve, Fig. 1b). Then the curves for each cell were fit with the Boltzmann function from  $-60$  mV to  $+50$  mV. The  $V_{\text{rev}}$  values were obtained by a linear extrapolation of the fit on the  $V$ -axis. The fit parameters and current densities  $I_{\text{max}}$  are presented in Table 1. To account for a transfection-dependent variation of current density, we determined current density values from at least three different transfections for each channel type. All mutants revealed reduced current densities compared with WT. For R650H,  $I_{\text{max}}$  was reduced by 39%, for R1362H by 50%, for HH by 58%, for R1362G by 65% and for HG by 84%. In addition, D4 mutants revealed large right-shifts ( $+14$  mV for R1362H and  $+13$  mV for R1362G) and a reduction in slope of the  $I$ – $V$  curves (Fig. 1b, Table 1), as expected for a neutralisation of positive charges in the voltage sensors S4. The tendentially larger shifts observed in the double mutants ( $+26$  mV for HH and  $+16$  mV for HG) indicated positive interactions of the D4/S4 mutants with the D2/S4 mutant, as the D2/S4 mutant had only marginal effects alone. We tested WT and R650H for a possible protonation by decreasing the pH from 7.4 to 7.2. Mild acidification shifted the voltage-dependence ( $V_{1/2}$ ) for both channels to the right: WT—by 9 mV ( $17 \pm 1$  mV,  $N=4$ ) and R650H—by 19 mV ( $22 \pm 6$  mV,  $N=4$ ), so that the initial left-shift between WT and R650H disappeared. However, it is due to an unspecific mechanism rather than a protonation of amino acid residues in voltage sensors, as (1) both, WT and R650H, shifted the voltage dependence of activation to the right by pH decrease from 7.4 to 7.2 (if H650 were deprotonated at 7.4, mild protonation would shift the  $I$ – $V$  curve to the left and would not shift the voltage dependence of WT) and (2) at a pH of 7.4, R650H is shifted to the left compared with WT, but the slope of the  $I$ – $V$  curve is decreased (consistent with the data of other groups), suggesting the interference of conformational changes and a possible charge neutralisation at position 650. As we see

**Fig. 1** **a** Superimposed representative barium current traces elicited by a pulse of  $100$ -ms depolarisation from a  $-90$ -mV holding potential to  $+10$  mV in WT and the mutants. **b** Current–voltage ( $I$ – $V$ ) relationships. Barium currents were elicited by a series of  $100$ -ms depolarisations from  $-90$  mV to the voltages listed. Current amplitudes were then normalised to cell capacitance, plotted against test voltages and fit to a sigmoid function

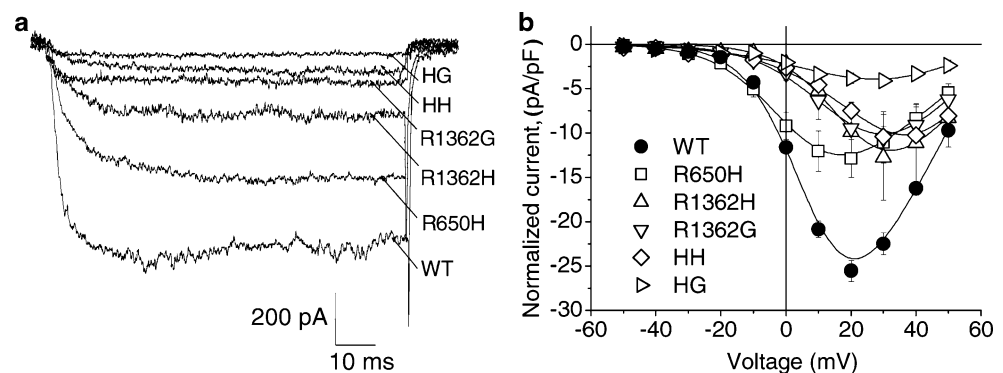


**Table 1** Current–voltage relationships and current density

	WT	R650H	R1362H	R1362G	HH	HG
$V_{1/2}$ (mV)	8.4±0.8	2.7±2.9*	22.2±1.7***	21.2±1.2***	34.3±3.4***	25.0±4.4***
$k$	-7.7±0.3	-9.6±1.0*	-9.9±0.9*	-12.7±1.7***	-12.7±0.8***	-15.0±1.0***
$V_{rev}$ (mV)	63.4±0.7	66.2±1.6	68.8±1.7**	69.5±4.7	66.2±1.9	65.5±5.6
$I_{max}$ (pA/pF)	-25.6±1.2	-15.6±2.6**	-12.8±4.8**	-9.0±2.6***	-10.7±0.6***	-4.2±0.5***
$N$	10	5	6	4	6	5

Fit parameters of the  $I$ - $V$  curves presented in Fig. 1b. The sigmoid fit function was  $I(V) = \frac{g_{max}(V-V_{rev})}{1+\exp\left(\frac{V-V_{1/2}}{k}\right)}$  where  $g_{max}$  is the conductance,  $V$  is the test voltage,  $V_{rev}$  is the reversal potential,  $V_{1/2}$  is the half-maximal voltage of activation and  $k$  is the slope.  $I_{max}$  is the current density (maximal current divided by the cell capacitance) and  $N$  is the number of cells.

\* $P<0.05$ ; \*\* $P<0.01$ ; \*\*\* $P<0.001$  are the significance levels.

from the global fitting data, R650H slows all gating transitions, implying the unspecific conformational changes to prevail over effective charge changes in a result of the R650H substitution. In general, our results suggest a more prominent role of the D4/S4 voltage sensor in the activation process compared with the D2/S4 segment.

#### Model of $Ca_v1.2$ gating

For the global fitting procedure, we needed to create a gating model, which satisfactorily fits both wild-type and mutant currents at all potentials. Common questions arising are (1) an existence of multiple open states [9, 14, 42] and (2) an evidence for multiple closed states [5, 11, 17, 30]. To answer these questions, we tested several models for their suitability in fitting ionic currents.

Our data could not be satisfactorily fit with any model containing only one open state (Fig. 2, left column), as such model failed to fit the second component of activation (Fig. 2, left column, arrows). Two open states were sufficient to account for the activation behaviour of our channels (Fig. 2, middle column). As the inactivation of the channels was incomparably slower than all other transitions, and in order not to bias our analysis, we assumed the inactivation to occur from both open states in our model.

Calcium channels, as other voltage-gated cation channels, were suggested to pass a series of non-conducting (closed) states before channel opening; however, different numbers of closed states were proposed for  $Ca^{2+}$  channel gating [5, 11, 17, 30]. Considering channel structure where four voltage sensors are thought to move upon membrane depolarisation [3], analogously to other voltage-gated cation channels [24] and as the model with four closed states (Fig. 2, middle column) could better account for the delay in current activation than the models with a lesser number of closed states (Fig. 2, right column), we introduced four closed states into our model.

The original model proposed by Hodgkin and Huxley [15], which is based on the independent operation of four voltage sensors, does not account for the details of activation when

data of macroscopic currents are complemented with single-channel and gating current recordings. In addition, the progression of the transition rates from the most closed states to the open state does not follow the predicted 4,3,2,1 ratios calculated from the progress of four identical independent subunits (for review, see [3]). As voltage sensors in voltage-gated cation channels do not move independently [3, 6, 43], we set the transition rates equal in the  $C_1 \leftrightarrow C_2 \leftrightarrow C_3 \leftrightarrow C_4 \leftrightarrow O_1$  pathway (Fig. 2, top), assuming cooperativity in voltage sensors movements [7, 24, 43].

#### Domain-specific effects of the mutations on $Ca^{2+}$ channel activation

To better resolve specific effects of the mutants studied on  $Ca^{2+}$  channel gating, we performed a simultaneous fit of current traces at seven different potentials to the model presented on Fig. 2 (middle column). Fit results are given in Table 2 and in the text.

The HypoPP mutations revealed domain-specific effects on  $Ca^{2+}$  channel gating. The D2/S4 mutation R650H symmetrically decreased both activation  $\alpha'_1$  and deactivation  $\beta'_1$  rates by approximately two times (Table 2), suggesting a symmetrical increase in the barrier height during transitions in either direction. Therefore, the equilibrium between C–C and C–O is reached more slowly. However, the equilibrium levels between adjacent states in the activation pathway  $C_1 \leftrightarrow C_2 \leftrightarrow C_3 \leftrightarrow C_4 \leftrightarrow O_1$ , determined as  $\alpha_1/\beta_1$  and, thus, the Gibbs energies  $\Delta G$ , remained almost the same as for the WT, explaining why there is only a small displacement of the  $I$ - $V$  curve along the  $V$ -axis (Fig. 1b, Table 1).

The D4/S4 mutants and the double mutants increased activation rates  $\alpha'_1$  up to two times (except R1362H, which was similar to WT) and deactivation rates  $\beta'_1$  up to three times (Table 2), reflecting a decreased barrier height and resulting in faster transitions. This change in barrier height is asymmetrical and results not only in kinetic changes (faster activation and deactivation), but also in different equilibrium levels. As the increase in rate constants was more prominent for deactivation than for activation (Table 2), the equilibrium

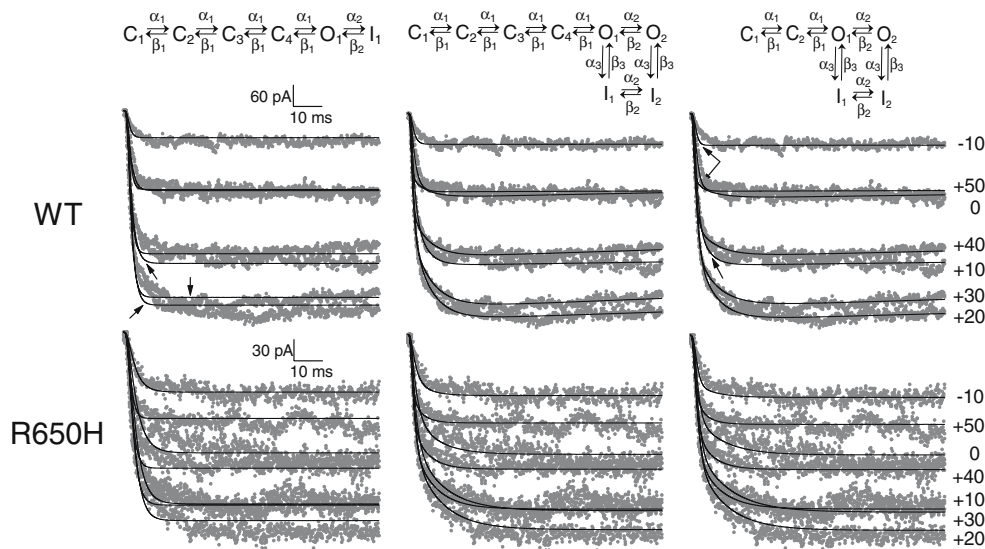


**Fig. 2** Choosing the model. As an example, representative ionic currents of WT (middle) and R650H mutation (bottom) are demonstrated. Ionic currents (shown in dots) elicited from a holding potential of  $-90$  mV by the voltages indicated (right) were simultaneously fit to the gating model presented on the top of the picture. Fits are overlaid (shown in lines). Arrows near the traces demonstrate a mismatch of fit and experimental

levels ( $\alpha_1/\beta_1$ ) were reduced at  $0$  mV from  $1.03$  (WT) to  $0.58$  (R1362H),  $0.70$  (R1362G),  $0.52$  (HH) or  $0.73$  (HG). As a result, Gibbs energy ( $\Delta G$ ) values between the states in the  $C_1 \leftrightarrow C_2 \leftrightarrow C_3 \leftrightarrow C_4 \leftrightarrow O_1$  pathway were less negative, resulting in a shift of the equilibrium to the earlier states and in impaired activation. This indicates that the activation pathway is disfavored due to disproportionally increased deactivation rate constants  $\beta_1$ . Macroscopically, it is reflected in the right-shifts of the  $I-V$  curves.

#### HypoPP-1 mutants reduce effective charge in the entire activation pathway

As the mutants neutralised gating charges in a voltage sensor, effective charge moving in the activation pathway (calculated

data. The model presented in the middle was selected for kinetic simulations. Sequential simplified models used for kinetic simulations (top):  $C_1-C_4$  are the closed states,  $O_1$  and  $O_2$  are the open states,  $I_1$  and  $I_2$  are the inactivated states reached from  $O_1$  and  $O_2$ , respectively,  $\alpha_1, \alpha_2, \alpha_3$  and  $\beta_1, \beta_2, \beta_3$  are the voltage-dependent transition rates between the states, as indicated in the models

as  $zx_{\alpha} + zx_{\beta}$ ) was decreased for all transitions ( $C_1 \rightarrow C_2 \rightarrow C_3 \rightarrow C_4 \rightarrow O_1$  and  $O_1 \rightarrow O_2$ ) (Table 2). As a consequence, the voltage dependence is reduced, most prominently in the double mutants, as more charge is neutralised (Table 2). Reduced voltage dependence is macroscopically reflected in the decreased slope of the  $I-V$  curves (Fig. 1b, Table 1). Based on the  $zx$  values for the mutants and WT (Table 2), we conclude that (1) most charge moves after the barrier peak and, therefore, only a small translocation of charge is needed to initiate an activation and a transition to the second open state  $O_2$  and vice versa, a large charge translocation is necessary for deactivation and  $O_2 \rightarrow O_1$  transition and (2) HypoPP mutations reduce mainly the part of the charge, which moves after the barrier peak is reached, thus reducing the voltage dependence of backward transitions—deactivation and  $O_2 \rightarrow O_1$ .

**Table 2** Activation pathway parameters

Parameters		WT	R650H	R1362H	R1362G	HH	HG
Activation	$\alpha'_1, s^{-1}$	$1,998 \pm 103$	$1,363 \pm 96^{**}$	$1,665 \pm 190$	$4,148 \pm 302^{***}$	$2,478 \pm 198^*$	$3,072 \pm 149^{***}$
	$\beta'_1, s^{-1}$	$1,934 \pm 126$	$1,256 \pm 238^*$	$2,885 \pm 290^{**}$	$5,939 \pm 332^{***}$	$4,783 \pm 122^{***}$	$4,185 \pm 125^{***}$
	$zx_{\alpha 1}$	$0.17 \pm 0.04$	$0.17 \pm 0.04$	$0.24 \pm 0.08$	$0.19 \pm 0.04$	$0.04 \pm 0.01^*$	$0.18 \pm 0.05$
$O_1-O_2$ transitions	$zx_{\beta 1}$	$0.92 \pm 0.07$	$0.77 \pm 0.19$	$0.46 \pm 0.09^{**}$	$0.50 \pm 0.12^*$	$0.51 \pm 0.03^{**}$	$0.36 \pm 0.07^{***}$
	$\alpha'_2, s^{-1}$	$122 \pm 7$	$56 \pm 12^{***}$	$144 \pm 20$	$119 \pm 13$	$99 \pm 10$	$100 \pm 10$
	$\beta'_2, s^{-1}$	$405 \pm 42$	$78 \pm 10^{***}$	$142 \pm 10^{***}$	$294 \pm 45$	$116 \pm 15^{***}$	$804 \pm 213^*$
	$zx_{\alpha 2}$	$0.21 \pm 0.06$	$0.20 \pm 0.18$	$0.75 \pm 0.39$	$0.35 \pm 0.16$	$0.63 \pm 0.08^{**}$	$0.12 \pm 0.05$
	$zx_{\beta 2}$	$2.6 \pm 0.1$	$0.7 \pm 0.2^{***}$	$0.8 \pm 0.3^{***}$	$0.3 \pm 0.1^{***}$	$0.2 \pm 0.2^{***}$	$0.6 \pm 0.4^{***}$

Activation pathway parameters obtained by global fitting of whole-cell currents to the kinetic model in Fig. 2 (middle column). Parameters  $\alpha'$  and  $\beta'$  were the corresponding forward and backward transition rate constants at  $0$  mV and are dependent on the entropy and enthalpy of the system. Parameters  $zx$  were the valences of the corresponding transitions and reflect voltage dependence of transition rates. Please refer to “Materials and methods” section for more details. Number of cells used in the global fitting: WT—10, R650H—5, R1362H—6, R1362G—3, HH—5 and HG—5. \* $P < 0.05$ ; \*\* $P < 0.01$ ; \*\*\* $P < 0.001$  are the significance levels.

## Effects of the HypoPP-1 mutations on the open states

The D2 R650H mutant revealed a specific effect on the transitions between the two open states  $O_1 \leftrightarrow O_2$ . Both forward  $\alpha_2$  and backward  $\beta_2$  transition rates were decreased (Table 2), suggesting increased barrier height between both states. This resulted in slower  $O_1 \leftrightarrow O_2$  transitions and in a long time ( $\tau = \frac{1}{\alpha_2 + \beta_2}$ ) to reach the equilibrium between the open states. The equilibrium level  $\alpha_2/\beta_2$  for R650H was more than two times increased compared to the WT (0.72 (R650H) vs 0.30 (WT)). As a result of the changed transition rates  $\alpha_2$  and  $\beta_2$ , the open probability in the second open state,  $P(O_2)$ , was mildly increased (Fig. 3d). However, the time to reach the equilibrium in the entire activation pathway, from  $C_1$  to  $O_2$ , was longer in R650H compared with WT, resulting in a slower activation.

The other mutants showed no change in  $\alpha_2$  level, but had a different impact on the  $O_2 \rightarrow O_1$  return rate  $\beta_2$ : for R1362H and HH, the  $\beta_2$  rate at 0 mV was approximately three times reduced, for R1362G unchanged and for the HG mutant two times increased (Table 2). The asymmetrical effects on the  $O_1 \leftrightarrow O_2$  transitions lead to a higher  $\Delta G$  between the open states favoring the transition to  $O_2$  in the R650H, R1362H and HH mutants. The calculated time fraction  $p$  spent in  $O_2$  was approximately two times increased in R650H, R1362H and HH mutants, pointing at re-distribution of the open states favoring  $O_2$  (Fig. 3d). This re-distribution of the open states is mainly realised by higher open probability  $P(O_2)$  in R650H and lower  $P(O_1)$  in R1362H and HH mutants (Fig. 3d). In R1362G and HG mutants, the distribution of the open states was similar to

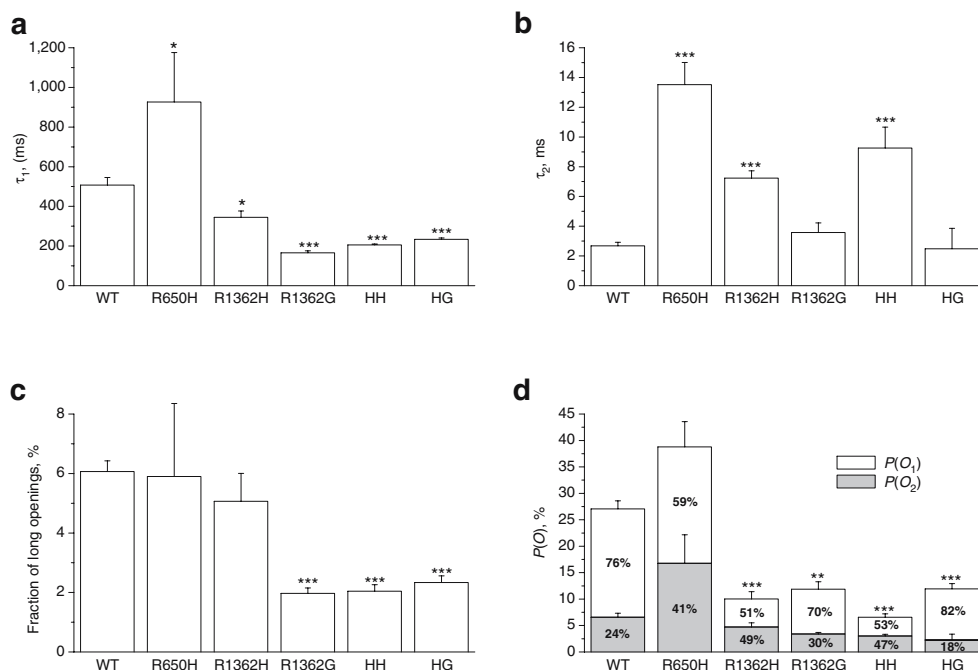
WT, suggesting conformational factors at position 1,362 playing a role in formation of the second open state.

Mutant-specific effects on the transitions in the  $C_1 \leftrightarrow C_2 \leftrightarrow C_3 \leftrightarrow C_4 \leftrightarrow O_1 \leftrightarrow O_2$  pathway, described here, are reflected in changed open state parameters. The  $O_1$  mean dwell time  $\tau(O_1)$  was  $\sim 2$  times increased in the R650H mutant. All other mutants revealed two to three times decreased  $\tau(O_1)$  due to increased deactivation forcing channels to close more rapidly (Fig. 3a). The  $O_2$  dwell time  $\tau(O_2)$  was increased 5 times in R650H, 2.7 times in R1362H and 3.4 times in HH, compared with WT (Fig. 3b). The  $O_2$  opening probability  $\xi(O_2)$  was  $\sim 3$  times reduced in R1362G and in the double mutants (Fig. 3c). All these changes lead to a reduced open probability  $P(O_1)$  and resulted in (1) the re-distribution of the open states in the histidine mutants, as discussed before, and (2) a significantly ( $P < 0.05$ ) lower total open probability  $P(O)$  in the D4/S4 HypoPP-1 mutants (Fig. 3d), suggesting “loss-of-function” mechanism of pathogenesis.

## Cooperativity between D2/S4 and D4/S4 mutations during activation

To estimate the cooperativity between the D2/S4 and D4/S4 mutations, we performed double-mutant cycle analysis. For both HH and HG mutants, there was no coupling in the  $C_1 \leftrightarrow C_2 \leftrightarrow C_3 \leftrightarrow C_4 \leftrightarrow O_1$  pathway ( $\Delta G_{\text{coupling}}$  in kcal/mol:  $0.14 \pm 0.13$  in HH,  $-0.07 \pm 0.13$  in HG), meaning that the effects of single mutations were additive in the double mutants. However, for the HH mutant, there was a negative coupling energy  $\Delta G_{\ddagger\text{coupling}}$  in activation  $\alpha_1$  ( $-0.47 \pm 0.11$  kcal/mol)

**Fig. 3** Characteristics of the open states. **a** Mean dwell time  $\tau$  in  $O_1$ . **b** Mean dwell time  $\tau$  in  $O_2$ . **c** Fraction of long openings  $\xi(\text{long})$  in % of all openings. **d** Probability  $P$  to be in a particular open state (given in parentheses) in equilibrium reflecting the fraction of total observation time spent in this open state.  $P(O)$  is a total open probability calculated as the sum of  $P(O_1)$  and  $P(O_2)$ . Values inside the columns reflect a proportion of time spent in  $O_1$  and  $O_2$ ,  $p(O_1)$  and  $p(O_2)$ , respectively. All parameters were calculated from fit results, as described in the “Materials and methods” section, number of cells is given in the legend to Table 2. Calculations were done at 0 mV in equilibrium. Significance levels are: \* $P < 0.05$ ; \*\* $P < 0.01$ ; \*\*\* $P < 0.001$



and deactivation  $\beta_1$  rate constants ( $-0.61 \pm 0.17$  kcal/mol), suggesting enhanced effects on the barrier height, although the final  $\Delta G_{\text{coupling}}$  did not change. In our case (Table 2), the activation and deactivation rate constants in HH were faster than the sum of effects of the single HypoPP-1 mutations, pointing to a non-additive barrier height decrease and, thus, a disproportional acceleration of kinetics in the HH mutant.

In the  $O_1 \leftrightarrow O_2$  transitions, there was a positive coupling energy  $\Delta G_{\text{coupling}}$  in the double mutants in equilibrium (HH:  $0.50 \pm 0.22$  kcal/mol; HG:  $1.50 \pm 0.36$  kcal/mol), suggesting the mutual attenuation of the effects of the single mutants. This  $\Delta G_{\text{coupling}}$  originated from a negative coupling energy  $\Delta G_{\ddagger, \text{coupling}}$ , unequal in forward ( $\alpha_2$ ) (HH:  $-0.32 \pm 0.19$  kcal/mol; HG:  $-0.39 \pm 0.17$  kcal/mol) and backward ( $\beta_2$ ) (HH:  $-0.82 \pm 0.15$  kcal/mol; HG:  $-1.40 \pm 0.29$  kcal/mol) transitions.

Negative coupling energy in the  $\alpha_1$  (HH) and  $\alpha_2$  (HH and HG) transitions is reflected in the fast kinetics of the double mutants, although the R650H mutant has the slower kinetics. This reveals dominant effects of the D4/S4 mutations on kinetics of the double mutants and suggests different roles of D2/S4 and D4/S4 voltage sensors in the gating of voltage-gated calcium channels.

## Discussion

Rationale for the selection of isoforms, expression system and charge carrier

Due to the unsolved problem of a sufficiently high expression of human  $Ca_v1.1$ , the few previous functional studies on HypoPP-1 mutations were performed using various channel isoforms, species and expression systems: the rabbit skeletal muscle  $\alpha_1$  subunit  $Ca_v1.1$ , the full form expressed in a muscular dysgenesis mouse (mdg) cell line (GLT) [23] and mouse fibroblast  $Ltk^-$  cells [26] or the truncated form expressed in *Xenopus* oocytes [32], the rabbit cardiac muscle  $\alpha_1$  subunit  $Ca_v1.2$  expressed in HEK293 cells [29] and myotubes cultured from satellite cells of patients [28, 31]. At the first glance, the patients' myotubes seem to be the best system but demonstrate, as immature cells, an expression profile differing from adult skeletal muscle; e.g. the L-type currents are superimposed by other calcium currents [28, 36]. Oocytes, used by another group [32], as a non-mammalian expression system, have a clearly different secondary modification.

In this study, we expressed the rabbit cardiac isoform in HEK293 cells, as done previously by Lerche et al. [29]. Decisively, expression levels of the cardiac isoform are higher than those of the skeletal muscle isoform, enabling a more accurate analysis of channel gating. Due to the high homology of the mutated S4 segments, previous results on

the HypoPP-1 mutations were similar in the skeletal muscle [31] and cardiac [29] isoforms, pointing at a similar function of the affected channel regions and making it possible to extrapolate the results from one isoform to another. Because the  $\beta_1$  subunit natively modulates the skeletal muscle but not the cardiac  $\alpha_1$  subunit, we co-expressed the  $\beta_2$  subunit that enhances  $\alpha_1$  subunit expression and thus produces measurable currents. In addition, we did not use the  $\alpha_2/\delta$  and  $\gamma$  subunits because transfection efficiency would be reduced and the co-transfection of these subunits did not significantly alter channel gating and the effects of HypoPP-1 mutations [29].

Finally, as the main goal of our study was to clarify the effects of the HypoPP-1 mutations on the transitions in the activation pathway, from the early closed to the open states, including the HypoPP impact on the balance between the open states, we used barium instead of calcium as charge carrier to avoid calcium-dependent inactivation. This type of inactivation, characteristic for some voltage-gated calcium channels, is in its nature different from other, kinetically distinct, voltage-dependent inactivation mechanisms (for review, see [13]). The presence of the both types of inactivation—voltage-dependent and calcium-dependent—would unnecessarily complicate our gating model, resulting in a range of additional fit parameters and, thus, degrees of freedom, masking the HypoPP-related effects and making our results less conclusive.

Global fitting procedure is a powerful tool for studying L-type  $Ca^{2+}$  channels

Previously, mainly two types of electrophysiological studies were performed on voltage-gated  $Ca^{2+}$  channels: either whole-cell currents were recorded and macroscopically analysed giving only a gross estimation of channel kinetics or single-channel currents were obtained, which enabled the analysis of open-time and opening frequency estimation, but not the evaluation of kinetic and thermodynamic characteristics of the gating transitions. In this study, we applied a global fitting procedure [1], which was successfully used to model the behaviour of different voltage-gated sodium [7, 24, 43] and potassium [18, 34] channels. This method yields a more precise picture of channel gating, especially the voltage dependency of a particular transition, the barrier height, equilibrium levels and the state distribution. Most importantly, using the global fitting procedure, we separated HypoPP-related effects on both components of activation and gained insight into all the steps of gating in WT and HypoPP-1 channels. Our results on relative proportions of the open states and values for the open-time constants for WT  $Ca_v1.2$  channels correspond well to the values obtained previously by single-channel measurements and fitting the channel open-time histograms [8, 19] supporting the reliability of our approach.

### All HypoPP mutations have “loss-of-function” features

Although causing the same disease, HypoPP-1 mutants in D2/S4 and D4/S4 affect channel gating in different ways. The main feature of the R650H mutant is slowing of all gating transitions—activation, deactivation, inactivation and between the open states. Previous macroscopic studies on this mutant in different calcium channel isoforms revealed small hyper-polarising shift of the  $I-V$  curve [23, 29, 32] and slowing of activation and deactivation rates [31, 32], fully in accordance with our data. Deceleration of all gating transitions in R650H implies the wide role of the D2/S4 segment in channel gating and suggests that the R650H mutation unspecifically hindered conformational changes associated with gating transitions.

In contrast, D4/S4 mutations (R1362H and R1362G) and the double mutations accelerated the activation transitions. However, they disfavored activation by disproportionately increasing deactivation rate constants, so that the equilibrium was shifted to preceding states. Previous study on D4/S4 mutants in *Xenopus* oocytes [32] demonstrated a right-shift of the activation curves and a strikingly faster deactivation as in our study; however, the authors reported slower activation rates. This seeming discrepancy emerged because the second open state whose fraction we showed to be two times increased in the D4/S4 mutants was not taken into account. As this second component of activation ( $O_1 \leftrightarrow O_2$ ) is tens of times slower than the fast component, an increased slow fraction makes the macroscopic activation appear slower, if fit with only one component.

Therefore, all HypoPP-1 mutations are “loss-of-function” mutations: D4/S4 mutations shift the equilibrium to the closed states, which results in smaller currents, and the D2/S4 mutant slows the activation. Similarly, sodium channel mutations causing HypoPP-2 were previously shown to have “loss-of-function” features [22, 25, 40]. In contrast to the HypoPP-1 mutations, which disfavor the activation pathway (this study), HypoPP-2 mutations increased channel unexcitability by stabilising the inactivated states [2, 25]. This divergence in mechanisms of action implies different roles of the S4 segments in the voltage-gated sodium and calcium channels.

### Second open state $O_2$ is favored in HypoPP-1 histidine mutations

HypoPP-1 mutants exhibited specific effects on channel open times in  $O_1$  and  $O_2$ , opening probability and time spent in each of the open states. Mean open time to  $O_1$  was increased in the R650H and reduced in the D4/S4, and in the double mutants, implying domain-specific effects determining the  $O_1$  mean lifetime and the strong dominant effect of the D4/S4 mutants leading to an intense  $O_1$  lifetime shortening in the double mutants.

The  $O_2$  lifetime was markedly increased in both histidine mutants and in the HH double mutant. This results in  $O_1-O_2$  re-distribution; whereas WT channels spend only 24% of the total open time in  $O_2$ , the histidine mutants reside 40–50% of the open time in  $O_2$ , i.e. these mutants spend equal time in both open states, although channel mean dwell times and opening probabilities may vary. In R1362G and HG mutants, the proportion of time spent in  $O_2$  was similar to WT. Our results suggest that (1) different domains play different roles in formation of the second open state in  $Ca^{2+}$  channels; (2) D4/S4 mutations have a dominant effect on  $O_2$  formation in the double mutants and (3) even at the same site, different amino acid substitutions can differently affect the  $O_1-O_2$  equilibrium. The second open state in this type of  $Ca^{2+}$  channel was suggested to be less selective for divalent cations, so that monovalent cations, such as  $Na^+$ , may be allowed to permeate the channel [20]. Therefore, the re-distribution of the open states towards  $O_2$  in HypoPP-1 lowered calcium channel selectivity.

Thus, there are two most important distinguishing characteristics of the HypoPP-1 mutants: (1) “loss-of-function” due to the suppressed activation and (2) the re-distribution of the open states. The latter, as a putative determinant of calcium channel selectivity, is of high physiological importance in HypoPP because the membrane depolarisation causing paralytic attacks in the HypoPP muscle is the result of shifts in the transmembrane gradients of electrolytes [33, 37, 38]. Therefore, we applied a calcium channel agonist ( $\pm$ )BayK8644 to reveal whether the function of the HypoPP-1 mutants is restored and how the open state distribution is affected in the WT and HypoPP-1 channels, as described in the companion paper by Kuzmenkin et al.

### D2/S4 vs D4/S4: specificity and cooperativity in $Ca^{2+}$ channel gating

As we demonstrated, the mutations in D2/S4 and D4/S4 differently affect channel gating. Their impact on channel activation, deactivation, inactivation and transitions between both open states suggests different roles of the D2/S4 and D4/S4 voltage sensors in channel gating. Mild changes of activation kinetics in D2/S4 R650H mutant imply a lesser role of D2/S4 segment in the  $Ca_v1.2$  activation process not only compared with D4/S4 voltage sensor, but also compared with the D2/S4 role in the voltage-gated sodium channels (for review, see [3]). Dominance of the effects of the D4 single mutations in D2/D4 double mutants reinforces this assumption. Residue-specific effects of the HypoPP-1 mutations point at conformational factors playing a role at the corresponding positions in voltage-gated  $Ca^{2+}$  channels.

**Acknowledgements** We thank Frank Lehmann-Horn for the helpful discussion and Simone Schatlowski for the technical assistance. This

work was supported by the German Research Foundation (DFG-JU470/1) and the IHP network on EC-coupling and calcium signaling in health and disease funded by the European Community.

### Appendix A

#### Kinetic simulations

For kinetic modelling, we created a new program (IonFit©) for global simultaneous fit of current traces. We fitted 7 current traces elicited by steps from a holding potential of -140 mV to the test potentials from -10 to +50 mV in 10-mV steps for each cell to the kinetic model presented in the Fig. 2, middle column. Goodness of fit was estimated from the  $\chi^2$  values.

The voltage-dependent forward  $\alpha$  and backward  $\beta$  transition rates between various states were assumed to be single exponential functions of voltage [39] and are given by

$$\alpha_1(V) = \alpha'_1 \exp\left(\frac{zX_{\alpha 1}FV}{RT}\right), \tag{1}$$

$$\beta_1(V) = \beta'_1 \exp\left(\frac{-zX_{\beta 1}FV}{RT}\right)$$

for the activation,

$$\alpha_2(V) = \alpha'_2 \exp\left(\frac{zX_{\alpha 2}FV}{RT}\right), \tag{2}$$

$$\beta_2(V) = \beta'_2 \exp\left(\frac{-zX_{\beta 2}FV}{RT}\right)$$

for the transitions between the open states  $O_1$  and  $O_2$  and

$$\alpha_3(V) = \alpha'_3 \exp\left(\frac{zX_{\alpha 3}FV}{RT}\right), \tag{3}$$

$$\beta_3(V) = \beta'_3 \exp\left(\frac{-zX_{\beta 3}FV}{RT}\right)$$

for the inactivation, as assigned in the model. As the voltage sensors in different domains do not move independently of each other [3, 6, 43] and analogously to previous results from other voltage-dependent cation channels [7, 24, 43], all transition rates in the activation pathway,  $C_1$  through  $O_1$ , were assumed to be equal. The fitted parameters were:  $\alpha'_1, \beta'_1, \alpha'_2, \beta'_2, \alpha'_3, \beta'_3$  for the transition rate constants including enthalpic and entropic factors; and  $zX_{\alpha 1}, zX_{\beta 1}, zX_{\alpha 2}, zX_{\beta 2}, zX_{\alpha 3}, zX_{\beta 3}$  for the valences of the corresponding forward and backward transitions. The latter reflected the effective charge moving from an original state to the barrier peak, as a product of the total charge moved and the fraction of the electric field where the barrier peak was located. Further parameters were  $V$ , the membrane potential;  $F$ , the Faraday constant;  $R$ , the gas constant and  $T$ , the absolute temperature.

Based on the fit parameters and according to our model, we estimated the mean channel dwell time  $\tau$  in  $O_1$  and in  $O_2$  as:

$$\tau(O_1) = \frac{1}{\alpha_2 + \alpha_3 + \beta_1}, \quad \tau(O_2) = \frac{1}{\alpha_3 + \beta_2}. \tag{4}$$

Furthermore, we estimated the probability  $P$  to be in any of the open states in equilibrium. According to the principle of detailed balance and our model, we had:  $K_{ij} = \frac{P(i)}{P(j)}$ , an equilibrium constant for any states  $i$  and  $j$  and

$$P(C_1) + P(C_2) + P(C_3) + P(C_4) + P(O_1) + P(O_2) = 1 \tag{5}$$

in the absence of inactivation.

Considering our model (Fig. 2, middle column) and according to Eq. (5), we obtained:

$$P(O_1) = \frac{\left(\frac{\alpha_1}{\beta_1}\right)^4}{1 + \frac{\alpha_1}{\beta_1} + \left(\frac{\alpha_1}{\beta_1}\right)^2 + \left(\frac{\alpha_1}{\beta_1}\right)^3 + \left(\frac{\alpha_1}{\beta_1}\right)^4 + \left(\frac{\alpha_1}{\beta_1}\right)^4 \frac{\alpha_2}{\beta_2}}, \tag{6}$$

$$P(O_2) = \frac{\left(\frac{\alpha_1}{\beta_1}\right)^4 \frac{\alpha_2}{\beta_2}}{1 + \frac{\alpha_1}{\beta_1} + \left(\frac{\alpha_1}{\beta_1}\right)^2 + \left(\frac{\alpha_1}{\beta_1}\right)^3 + \left(\frac{\alpha_1}{\beta_1}\right)^4 + \left(\frac{\alpha_1}{\beta_1}\right)^4 \frac{\alpha_2}{\beta_2}},$$

$$P(O) = P(O_1) + P(O_2),$$

where  $P(O_1)$  and  $P(O_2)$  are the probabilities to be in  $O_1$  and  $O_2$ , respectively, and  $P(O)$  the probability to be in any of the open states. Thus,  $P(O)$  corresponds to the time fraction of the openings in single-channel measurements.

As a special case of Eqs. (5) and (6), we estimated the  $O_1$ - $O_2$  distribution by calculating the fractions of open time  $p$  spent in a particular open state. Contrary to Eq. (5), we considered only the equilibrium between the open states in the absence of any other transitions:

$$\frac{p(O_2)}{p(O_1)} = \frac{\alpha_2}{\beta_2}, \quad p(O_1) + p(O_2) = 1 \tag{7}$$

where  $p(O_1)$  and  $p(O_2)$  are fractions of time spent in  $O_1$  and  $O_2$ , respectively.

Solving this equation system, we obtained:

$$p(O_1) = \frac{\beta_2}{\alpha_2 + \beta_2}, \quad p(O_2) = \frac{\alpha_2}{\alpha_2 + \beta_2}. \tag{8}$$

Further, we estimated the fractions of long and short openings  $\xi$ . In this study, we performed our calculations in the absence of inactivation, as the inactivation rates  $\alpha_3$  were incomparably slower than the other transitions. Considering a channel being in  $O_1$  and comparing a probability to pass

to O<sub>2</sub> (long opening) with a probability to close (short opening), and as

$\xi(\text{long}) \sim \alpha_2$ ,  $\xi(\text{short}) \sim \beta_1$ ,  $\xi(\text{long}) + \xi(\text{short}) = 1$ , we obtained:

$$\xi(\text{long}) = \frac{\alpha_2}{\alpha_2 + \beta_1}, \quad \xi(\text{short}) = \frac{\beta_1}{\alpha_2 + \beta_1}. \quad (9)$$

## Appendix B

### Double-mutant cycle analysis

For the estimation of cooperativity of the HypoPP-1 D2/S4 and D4/S4 mutations in all the transitions in Ca<sup>2+</sup> channel gating, we used a thermodynamic description of mutant-specific effects. We calculated the free energy change due to a transition between the channel states as

$$\Delta G(V) = -RT \ln \frac{\alpha_x(V)}{\beta_x(V)},$$

where  $x=1$  for C $\leftrightarrow$ C and C $\leftrightarrow$ O transitions,  $x=2$  for O<sub>1</sub> $\leftrightarrow$ O<sub>2</sub> transitions and  $x=3$  for O $\leftrightarrow$ I transitions.  $\Delta G$  is the difference in free energy between the states in the equilibrium and is not sensitive to symmetrical changes in barrier height, which do not change the equilibrium level  $\alpha/\beta$ , but only change the rate of reaching it. In the two-state system this rate is determined as  $\alpha + \beta$ . To solve the problem, we further estimated a free energy change from a state of origin to a peak of the energy barrier between states. Considering  $\alpha_x = \nu \exp\left(-\frac{\Delta G_{\ddagger}^{\alpha}}{RT}\right)$  and  $\beta_x = \nu \exp\left(-\frac{\Delta G_{\ddagger}^{\beta}}{RT}\right)$  where  $\nu$  is a pre-factor, we obtained  $\Delta G_{\ddagger}^{\alpha}(V) = -RT \ln \alpha_x(V) + RT \ln \nu$  for any forward transition and  $\Delta G_{\ddagger}^{\beta}(V) = -RT \ln \beta_x(V) + RT \ln \nu$  for any backward transition.

To measure the effect of a mutant on any channel gating transition, we calculated the difference between the corresponding  $\Delta G$  values:

$$\Delta \Delta G_{\text{WT} \rightarrow \text{MUT}}(V) = \Delta G_{\text{MUT}}(V) - \Delta G_{\text{WT}}(V)$$

For the calculation of  $\Delta \Delta G^{\alpha}$  and  $\Delta \Delta G^{\beta}$ , we assumed the pre-factor  $\nu$  to be equal for the WT and the mutant channels. If there is no coupling between two mutations, the change in free energy associated with a transition upon a double mutation equals the sum of changes in free energy due to the single mutations. The deviation from the additivity is the coupling energy between the two mutations in a particular transition [16]:

$$\Delta G_{\text{coupling}}(V) = \Delta \Delta G_{\text{WT} \rightarrow \text{MUT1}/\text{MUT2}}(V) - [\Delta \Delta G_{\text{WT} \rightarrow \text{MUT1}}(V) + \Delta \Delta G_{\text{WT} \rightarrow \text{MUT2}}(V)]$$

$\Delta G$  values were calculated for each cell separately and then averaged for a channel type. Also, we determined a voltage dependence of coupling energy. However, as it did not provide us with new information on channel gating and for simplicity, in the “Results” section, we present the coupling energy values calculated at 0 mV. Data are presented as the mean  $\pm$  standard error of the mean (SEM), the latter is calculated by error propagation.

## References

- Balsler JR, Roden DM, Bennett PB (1990) Global parameter optimization for cardiac potassium channel gating models. *Biophys J* 57:433–444
- Bendahhou S, Cummins TR, Griggs RC, Fu YH, Ptacek LJ (2001) Sodium channel inactivation defects are associated with acetazolamide-exacerbated hypokalemic periodic paralysis. *Ann Neurol* 50:417–420
- Bezanilla F (2000) The voltage sensor in voltage-dependent ion channels. *Physiol Rev* 80:555–592
- Bulman DE, Scoggan KA, van Oene MD, Nicolle MW, Hahn AF, Tollar LL, Ebers GC (1999) A novel sodium channel mutation in a family with hypokalemic periodic paralysis. *Neurology* 53:1932–1936
- Byerly L, Chase PB, Stimers JR (1984) Calcium current activation kinetics in neurones of the snail *Lymnaea stagnalis*. *J Physiol* 348:187–207
- Chanda B, Asamoah OK, Bezanilla F (2004) Coupling interactions between voltage sensors of the sodium channel as revealed by site-specific measurements. *J Gen Physiol* 123:217–230
- Chanda B, Bezanilla F (2002) Tracking voltage-dependent conformational changes in skeletal muscle sodium channel during activation. *J Gen Physiol* 120:629–645
- Erxleben C, Gomez-Alegria C, Darden T, Mori Y, Bimbaum L, Armstrong DL (2003) Modulation of cardiac Ca(V)1.2 channels by dihydropyridine and phosphatase inhibitor requires Ser-1142 in the domain III pore loop. *Proc Natl Acad Sci USA* 100:2929–2934
- Fass DM, Levitan ES (1996) L-type Ca<sup>2+</sup> channels access multiple open states to produce two components of Bay K 8644-dependent current in GH3 cells. *J Gen Physiol* 108:13–26
- Fleig A, Takeshima H, Penner R (1996) Absence of Ca<sup>2+</sup> current facilitation in skeletal muscle of transgenic mice lacking the type 1 ryanodine receptor. *J Physiol* 496:339–345
- Forti L, Pietrobon D (1993) Functional diversity of L-type calcium channels in rat cerebellar neurons. *Neuron* 10:437–450
- Hamill OP, Marty A, Neher E, Sakmann B, Sigworth FJ (1981) Improved patch-clamp techniques for high-resolution current recording from cells and cell-free membrane patches. *Pflugers Arch* 391:85–100
- Hering S, Berjukow S, Sokolov S, Marksteiner R, Weiss RG, Kraus R, Timin EN (2000) Molecular determinants of inactivation in voltage-gated Ca<sup>2+</sup> channels. *J Physiol* 528:237–249
- Hess P, Lansman JB, Tsien RW (1984) Different modes of Ca channel gating behaviour favoured by dihydropyridine Ca agonists and antagonists. *Nature* 311:538–544
- Hodgkin AL, Huxley AF (1952) A quantitative description of membrane current and its application to conduction and excitation in nerve. *J Physiol* 117:500–544
- Horovitz A, Fersht AR (1990) Strategy for analysing the cooperativity of intramolecular interactions in peptides and proteins. *J Mol Biol* 214:613–617

17. Jafri MS, Rice JJ, Winslow RL (1998) Cardiac Ca<sup>2+</sup> dynamics: the roles of ryanodine receptor adaptation and sarcoplasmic reticulum load. *Biophys J* 74:1149–1168
18. Johnson JP Jr, Balsler JR, Bennett PB (2001) A novel extracellular calcium sensing mechanism in voltage-gated potassium ion channels. *J Neurosci* 21:4143–4153
19. Josephson IR, Guia A, Lakatta EG, Stern MD (2002) Modulation of the gating of unitary cardiac L-type Ca(2+) channels by conditioning voltage and divalent ions. *Biophys J* 83:2575–2586
20. Josephson IR, Guia A, Lakatta EG, Stern MD (2002) Modulation of the conductance of unitary cardiac L-type Ca(2+) channels by conditioning voltage and divalent ions. *Biophys J* 83:2587–2594
21. Jurkat-Rott K, Lehmann-Horn F, Elbaz A, Heine R, Gregg RG, Hogan K, Powers PA, Lapie P, Vale-Santos JE, Weissenbach J et al (1994) A calcium channel mutation causing hypokalemic periodic paralysis. *Hum Mol Genet* 3:1415–1419
22. Jurkat-Rott K, Mitrovic N, Hang C, Kouzmekine A, Iaizzo P, Herzog J, Lerche H, Nicole S, Vale-Santos J, Chauveau D, Fontaine B, Lehmann-Horn F (2000) Voltage-sensor sodium channel mutations cause hypokalemic periodic paralysis type 2 by enhanced inactivation and reduced current. *Proc Natl Acad Sci USA* 97:9549–9554
23. Jurkat-Rott K, Uetz U, Pika-Hartlaub U, Powell J, Fontaine B, Melzer W, Lehmann-Horn F (1998) Calcium currents and transients of native and heterologously expressed mutant skeletal muscle DHP receptor alpha1 subunits (R528H). *FEBS Lett* 423:198–204
24. Kuzmenkin A, Bezanilla F, Correa AM (2004) Gating of the bacterial sodium channel, NaChBac: voltage-dependent charge movement and gating currents. *J Gen Physiol* 124:349–356
25. Kuzmenkin A, Muncan V, Jurkat-Rott K, Hang C, Lerche H, Lehmann-Horn F, Mitrovic N (2002) Enhanced inactivation and pH sensitivity of Na(+) channel mutations causing hypokalemic periodic paralysis type II. *Brain* 125:835–843
26. Lapie P, Goudet C, Nargeot J, Fontaine B, Lory P (1996) Electrophysiological properties of the hypokalemic periodic paralysis mutation (R528H) of the skeletal muscle alpha 1s subunit as expressed in mouse L cells. *FEBS Lett* 382:244–248
27. Lehmann-Horn F, Jurkat-Rott K, Rudel R (2002) Periodic paralysis: understanding channelopathies. *Curr Neurol Neurosci Rep* 2:61–69
28. Lehmann-Horn F, Sipos I, Jurkat-Rott K, Heine R, Brinkmeier H, Fontaine B, Kovacs L, Melzer W (1995) Altered calcium currents in human hypokalemic periodic paralysis myotubes expressing mutant L-type calcium channels. *Soc Gen Physiol Ser* 50:101–113
29. Lerche H, Klugbauer N, Lehmann-Horn F, Hofmann F, Melzer W (1996) Expression and functional characterization of the cardiac L-type calcium channel carrying a skeletal muscle DHP-receptor mutation causing hypokalemic periodic paralysis. *Pflugers Arch* 431:461–463
30. Ma J, Gonzalez A, Chen R (1996) Fast activation of dihydropyridine-sensitive calcium channels of skeletal muscle. Multiple pathways of channel gating. *J Gen Physiol* 108:221–232
31. Morrill JA, Brown RH Jr, Cannon SC (1998) Gating of the L-type Ca channel in human skeletal myotubes: an activation defect caused by the hypokalemic periodic paralysis mutation R528H. *J Neurosci* 18:10320–10334
32. Morrill JA, Cannon SC (1999) Effects of mutations causing hypokalemic periodic paralysis on the skeletal muscle L-type Ca<sup>2+</sup> channel expressed in *Xenopus laevis* oocytes. *J Physiol* 520:321–336
33. Niall JF, Pak Poy RK (1966) Studies in familial hypokalemic periodic paralysis. *Australas Ann Med* 15:352–358
34. Olcese R, Latorre R, Toro L, Bezanilla F, Stefani E (1997) Correlation between charge movement and ionic current during slow inactivation in Shaker K<sup>+</sup> channels. *J Gen Physiol* 110:579–589
35. Ptacek LJ, Tawil R, Griggs RC, AG Engel, Layzer RB, Kwiecinski H, McManis PG, Santiago L, Moore M, Fouad G et al (1994) Dihydropyridine receptor mutations cause hypokalemic periodic paralysis. *Cell* 77:863–868
36. Rivet M, Cognard C, Imbert N, Rideau Y, Duport G, Raymond G (1992) A third type of calcium current in cultured human skeletal muscle cells. *Neurosci Lett* 138:97–102
37. Ruff RL, Gordon AM (1986) Disorders of muscle. The periodic paralyses. In: Andreoli TE, Hoffman JF, Fanestil DD, Schultz SG (eds) *Physiology of membrane disorders*, 2nd edn. Plenum, New York, NY, pp 825–839
38. Shy GM, Wanko T, Rowley PT, Engel AG (1961) Studies in familial periodic paralysis. *Exp Neurol* 3:53–121
39. Stevens CF (1978) Interactions between intrinsic membrane protein and electric field. An approach to studying nerve excitability. *Biophys J* 22:295–306
40. Struyk AF, Scoggan KA, Bulman DE, Cannon SC (2000) The human skeletal muscle Na channel mutation R669H associated with hypokalemic periodic paralysis enhances slow inactivation. *J Neurosci* 20:8610–8617
41. Stuhmer W, Conti F, Suzuki H, Wang XD, Noda M, Yahagi N, Kubo H, Numa S (1989) Structural parts involved in activation and inactivation of the sodium channel. *Nature* 339:597–603
42. Sun L, Fan JS, Clark JW, Palade PT (2000) A model of the L-type Ca<sup>2+</sup> channel in rat ventricular myocytes: ion selectivity and inactivation mechanisms. *J Physiol* 529:139–158
43. Vandenberg CA, Bezanilla F (1991) A sodium channel gating model based on single channel, macroscopic ionic, and gating currents in the squid giant axon. *Biophys J* 60:1511–1533